Adsorption performance of silver ion on acrylic grafted carboxymethyl chitosan/dialdehyde starch

Jinyu Ouyang[1] · Luqi Zhan[1] · Qincong Luo[1] · Jincheng Miao[1] · Langrong Hu[1] · Xiangqi He[1] · Xiaojuan Wang[1]

Abstract
In the present study, the novel environmental-friendly adsorbent (PAA-*g*-CMCDAS) obtained from carboxymethyl chitosan (CMC), dialdehyde starch (DAS) and polyacrylic acid (PAA) is used for removing silver ion. The adsorbent characterized by XRD, SEM, TGA, BET and FTIR, was evaluated for removal of silver ion from aqueous solution. The adsorption process of silver ions conformed to Langmuir isotherm and the second-order kinetic mode. The maximum adsorption capacity for silver ions was 404.77 mg·g^{-1}, and the maximum removal efficiency was 95.05%. Also, the reusability and selectivity of PAA-*g*-CMCDAS was investigated, and the adsorption amount was still 388.77 mg·g^{-1} and the removal efficiency was up to 91.29% after five times recycle; the removal efficiency of silver ions in mixed metal ions solution was 24.24% with the total removal efficiency of mixed metal ions 58%. Therefore, PAA-*g*-CMCDAS was an excellent silver ion adsorbent with good reusability.

Keywords Multi-modified starch · Silver · Selective adsorbent · Carboxymethyl chitosan · Acrylic acid

1 Introduction

The contamination of heavy metal ions has endangered human health and the environment, especially the security of food and agricultural threatened by silver wastewater [1–4], such as cancer, heart-failure and other diseases originated in the high concentration of silver ions in drinking water (exceeding 0.1 mg·L^{-1}) [5]. However, silver, a precious metal, possesses advantages such as antibacterial, antiviral, anti-inflammatory and high sensitivity, and has been widely used in biology [6], medicine [7] and other fields [8, 9]. Therefore, recovery of silver ions from wastewater has become an important task, which is beneficial to environmental safety and human health [10], and the need for effective methods and materials has increased. Studies on the recovery of silver ions by using different methods such as adsorption [11, 12], membrane separation [13] are available in the literature. Adsorption is the most effective method and needs suitable solid adsorbents with the desired chemical structure and geometry. Until now, different adsorbents have been prepared for recovery of silver ions, and the non-toxic bio-based adsorbent is one of the most studied [14–16].

Chitosan is a potential adsorbent according to its abundant amino and carboxyl groups [17, 18], and can cross link polyhydroxy-compound. Modified carboxymethyl chitosan exhibited better adsorption performance for Pb(II), Cu(II), Zn(II) and Au(I) [19, 20]. Carboxymethyl chitosan-sewage sludge bio-char revealed a shorter equilibrium time (< 60 min) for Pb(II) adsorption and a superior capacity of 594.17 mg·g^{-1} for Hg(II) adsorption [21]. The chitosan/bamboo charcoal composites had been used as Ag(I) adsorbent and its removal efficiency was almost up to 100% with 52.91 mg·g^{-1} of adsorption capacity [22], caused by the selective chelation between silver ion and amino/carboxyl groups.

Starch, the most abundant organic substance on the earth, has been modified to adsorb metal ions or dyes [23, 24], inhibit microorganisms and bacteria, etc [25]. Starch nanoparticles (SNPs) exhibited high adsorption capacities for Pb(II) and Cu(II) [26]. Starch modified by dibenzo-18-crown-6 was used to adsorb Cd(II), Zn(II), Ni(II) and Cu(II)

✉ Xiaojuan Wang
  wangxiaojuan0117@163.com

1 Guangxi Key Laboratory of Electrochemical and Magneto-chemical Function Materia, College of Chemistry and Bioengineering, Guilin University of Technology, Guilin 541004, China

from aqueous solution, and it is a good, reusable and highly efficient adsorbent for the removal of heavy metal ions from wastewater [27]. Dialdehyde starch, a selectively oxidized starch with abundant hydroxy and aldehyde groups, was always modified to adsorb metal ions [28–31], inhibit microorganisms and bacteria [32], crosslink materials [33], etc. Dialdehyde starch modified by Y-NH$_2$ compounds are effective ligands for metal ions such as Zn(II), Pb(II), Cu(II), Cd(II), and Ni(II) [30, 31].

Numerous studies have reported that modified chitosan and starch have been used in the adsorption of heavy metals due to its abundant functional groups and large surface area.

Acrylic acid is a monomer of polymerization with carboxyl groups and can chelate metal ions [34, 35]. Acrylamide/acrylic acid cellulose hydrogels were prepared to adsorb metal ions, and the maximum absorption capacity of Cu(II), Pb(II) and Cd(II) were 157.51, 393.28 and 289.97 mg·g^{-1}, respectively [36], which was attributed to the chelation between metal ions and the large carboxyl and amino groups on the surface of hydrogels.

In the present study, an effective and selective environmental-friendly adsorbent for silver ion was obtained by crosslinking of polyacrylic acid, carboxymethyl chitosan and dialdehyde starch. Both amine and carbonyl groups on the surface of the environmental-friendly adsorbent can selectively chelation with silver ion. The present study investigated the adsorption performance of the prepared environmental-friendly adsorbent for silver ions from aqueous solutions.

2 Experiment

2.1 Reagents

Corn starch (Food Grade) with M$_w$ $1 \times 10^5 \sim 1 \times 10^6$ was purchased from Longkou Wugu Food Co., Ltd. (China); carboxymethyl chitosan (AR) was purchased from Shanghai Yien Chemical Technology Co., LTD. (China); sodium periodate (AR, S817518-100 g) was purchased from Shanghai Macklin Biochemical Co., Ltd. (China); and silver nitrate (AR) was purchased from Sinopagic Chemical Reagent Co., LTD. (China). All other chemicals were of analytical reagents grades and purchased from Xilong Science Co., Ltd.

2.2 Synthesis of dialdehyde starch (DAS)

The synthesis process of dialdehyde starch (DAS) has been shown in Scheme 1 [32, 37]. Firstly, corn starch (15 g) and distilled water (150 mL) were added into a 250 mL three-necked round-bottomed flask. The mixture was stirred for 0.5 h at 25 °C. Secondly, a certain amount of sodium periodate was added into the corn starch solution, and the pH of the mixture was adjusted to 3.5. After the oxidation at 25 °C for 6 h, the suspension was filtered, and the precipitate was washed by deionized water and ethanol successively, and dried at 50 °C for 5 h. Finally, the content of aldehydes in DAS was determined by alkali loss method.

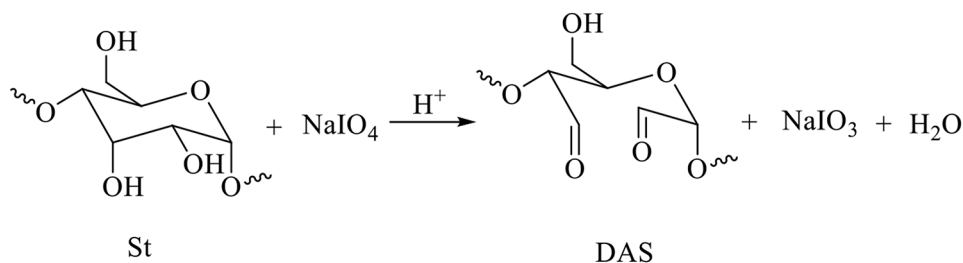### 2.3 Synthesis of carboxymethyl chitosan/ dialdehyde starch (CMCDAS)

The synthesis process of carboxymethyl chitosan/dialdehyde starch has been shown in Scheme 2. Firstly, dialdehyde starch and carboxymethyl chitosan were suspended in 10 times the isopropanol/water mixture (4:1) respectively. Secondly, carboxymethyl chitosan suspension was added into the suspension of dialdehyde starch at 50 ºC for 12 h. After the addition, the suspension was filtered, and the precipitate was washed by distilled water and methanol successively. Finally, the sample was obtained after drying at 50 ºC for 2 h in a vacuum drying oven.

The nitrogen content of CMCDAS was measured by *Kjeldahl* method [38] using a nitrogen analyzer (KDN-08 C(04 C), Shanghai Huarui Instrument Co., Ltd.) and calculated using the following equation (Eq. 1):

$$N\% = \frac{(V - V_0) \times N_0 \times 0.014 \times 100}{W_1} \tag{1}$$

where $N\%$ is the nitrogen content; N_0 is the molar concentration of standard sulfuric acid used for titration, mol·L^{-1}; V_0 is the volume of sulfuric acid standard solution used for blank determination, L; V is the volume of sulfuric acid

Scheme 1 Synthesis process of dialdehyde starch (DAS)

St

DAS

Scheme 2 Synthesis process of carboxymethyl chitosan/dialdehyde starch (CMCDAS)

DAS + CMC → CMCDAS
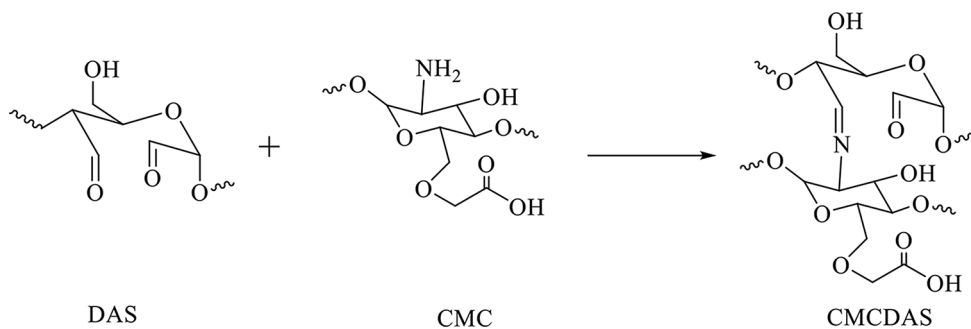
Scheme 3 Modification process of CMCDAS with acrylic (PAA-*g*-CMCDAS)

CMCDAS + AA → PAA-g-CMCDAS
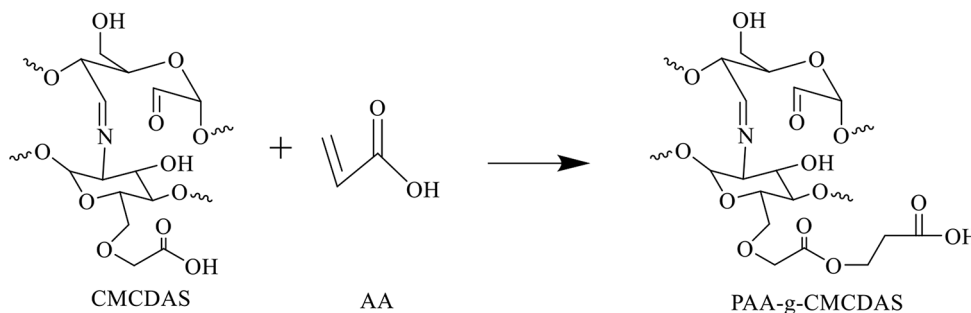
standard solution used for sample determination, L; and W_1 is the sample weight, g.

2.4 The modification process of CMCDAS with acrylic

The modification process of CMCDAS with acrylic was shown in Scheme 3 [39]. Firstly, CMCDAS (1 g) and distilled water (30 mL) were added into a 100 mL three-necked round-bottomed flask. The mixture was stirred for 0.5 h at 25 °C under nitrogen. Then, ammonium persulfate (0.1 g) was added into the flask with stir for 15 min. Secondly, acrylic acid (AA) and *N*, *N*'-methylenebisacrylamide (MBA, 0.1 g) was added, and the mixture was stirred and refluxed at 70 °C for 3 h. After being neutralized to pH = 7.0 by 1 mol·L^{-1} KOH, filtered, washed by distilled water and dried at 70 °C, the final product was defined to PAA-*g*-CMCDAS.

2.5 Characterizations

The samples were characterized by several instruments. Functional group analysis was attained by Fourier transform infrared spectrometer (FTIR, Nexus 470, Nicolet, USA) between wavelengths of 4000–500 cm^{-1} with 32-scans at room temperature and the resolution of 4 cm^{-1}. The morphological properties were obtained by field emission scanning electron microscopy (SEM, EDS, Hitachi 5V5000, Hitachi Hi-Tech Co., Ltd.) at the voltage of 5 kV and 15 kV. Thermogravimetric curves were obtained by thermogravimetric analyzer (TGA, SDT Q600, TA Instrument) at a 10

°C·min^{-1} heating rate in the range from 20 °C to 800 °C in the 100 mL·min^{-1} atmosphere of nitrogen. The specific surface properties were examined by the Specific surface area analyzer (BET, ASAP 2460, McMuritik, USA).

2.6 Adsorption process

The adsorption performance of PAA-*g*-CMCDAS on 0.05 mol·L^{-1} silver nitrate solution was studied as follows: (1) a certain dosage of adsorbent was added into 50 mL silver nitrate solution; (2) the adsorption process was sustained with continuous magnetically stir; (3) the supernatant which contained residual silver nitrate was obtained after standing 2 h. The concentration of residual silver nitrate was determined by plasma inductively coupled spectrometer (ICP, HKYT-799, Beijing), and then the adsorption capacity (Q) and the removal efficiency ($Q\%$) was calculated by the following equation (Eqs. 2 and 3) [40]:

$$Q = [(C_0 - C_i) \times V_i]/W_2 \tag{2}$$

$$Q\% = (C_0 - C_i)/C_0 \times 100\% \tag{3}$$

where Q is the adsorption capacity, mg·g^{-1}; $Q\%$ is the removal efficiency; C_0 is the initial concentration of silver nitrate solution, mg·L^{-1}; C_i is the concentration of silver nitrate solution after adsorption, mg·L^{-1}; V_i is the volume of solution, L; W_2 is the dosage of adsorbent, mg.

2.7 Reusability

The reusability of PAA-*g*-CMCDAS was evaluated by the removal of Ag(I) from silver nitrate solution with five cycles. Therefore, the Ag(I) on the PAA-*g*-CMCDAS were desorbed by 0.1 mol·L^{-1} NaCl for 1 h to regenerate the PAA-*g*-CMCDAS; and then the regenerated PAA-*g*-CMCDAS was filtrated under ordinary pressure. After repeated washing with distilled water and acetone, the filtrated PAA-*g*-CMCDAS was dried under infrared light. Finally, the dried PAA-*g*-CMCDAS was reused to adsorb Ag(I) in silver nitrate solution. Thereinto, the PAA-*g*-CMCDAS/Ag was the precipitate after first adsorption and the PAA-*g*-CMCDAS/mAg was the precipitate after five recycles.

3 Results and discussion

3.1 Characterization of adsorbent

The SEM images of corn starch (a), DAS (b), CMCDAS (c), PAA-*g*-CMCDAS (d), PAA-*g*-CMCDAS/Ag (e) and PAA-*g*-CMCDAS/mAg (f) were shown in Fig. 1. The surface of DAS was different with the round or irregular corn starch (a and b) [41]. The surface of PAA-*g*-CMCDAS (d) was irregular and obviously cross-linked, which was caused by the reaction of dialdehyde starch and carboxymethyl chitosan. The SEM images indicated that the oxidation and cross-linking reaction would gradually destroy the structure of corn starch granules and obviously enlarge the specific surface area of corn starch, which was beneficial to adsorbing metal ions [42].

The EDS images showed that: (1) a large amount of Ag(I) was on the surface of PAA-*g*-CMCDAS/Ag (Fig. 2a) and PAA-*g*-CMCDAS/mAg (Fig. 2b) respectively; (2) the content of Ag(I) on the surface of PAA-*g*-CMCDAS was more than 70%. These images indicated that PAA-*g*-CMCDAS absorbed a large amount of Ag(I) during the adsorption process, and the results of EDS were consistent with the SEM.

The XRD pattern of PAA-*g*-CMCDAS/mAg (Fig. 3), referring to the XRD pattern of AgCl standard, indicated that the adsorbed Ag(I) on the surface of PAA-*g*-CMCDAS was silver chloride formed by the silver ion and sodium chloride [12]. The results indicated that PAA-*g*-CMCDAS

Fig. 1 SEM image of ST (**a**), DAS (**b**), CMCDAS (**c**), PAA-*g*-CMCDAS (**d**), PAA-*g*-CMCDAS/Ag (**e**) and PAA-*g*-CMCDAS/mAg (**f**)
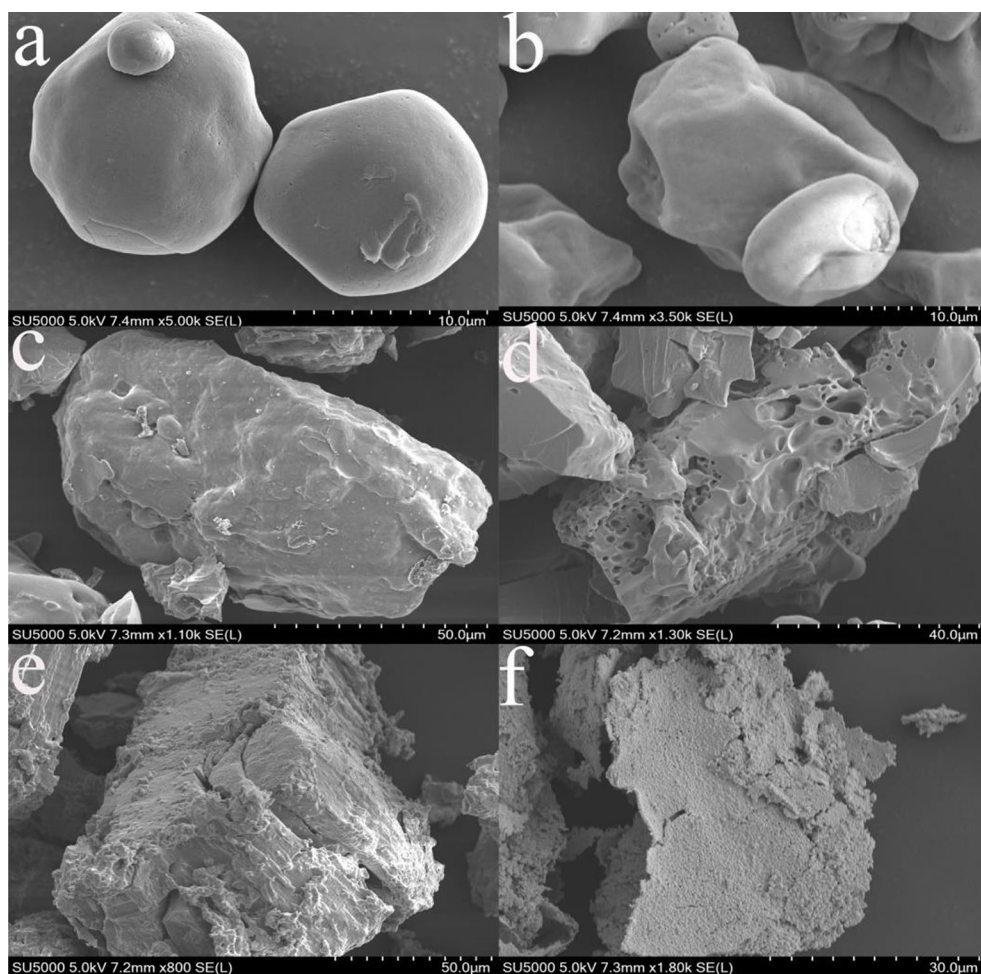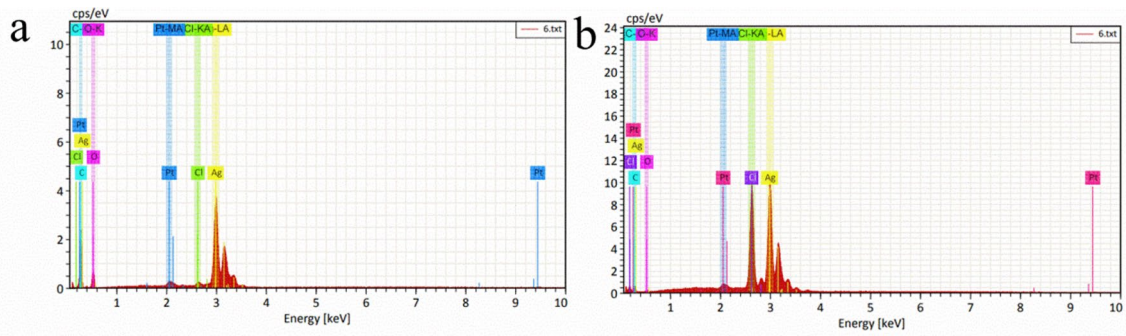
Fig. 2 The EDS image of PAA-*g*-CMCDAS/Ag (**a**) and PAA-*g*-CMCDAS/mAg (**b**)

Fig. 3 XRD patterns of PAA-*g*-CMCDAS/mAg
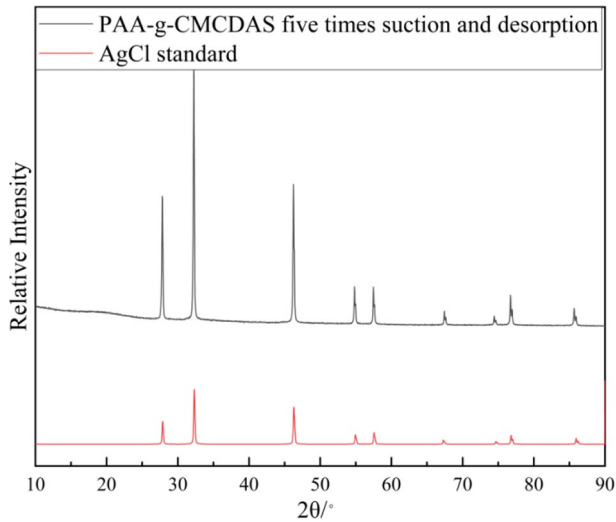

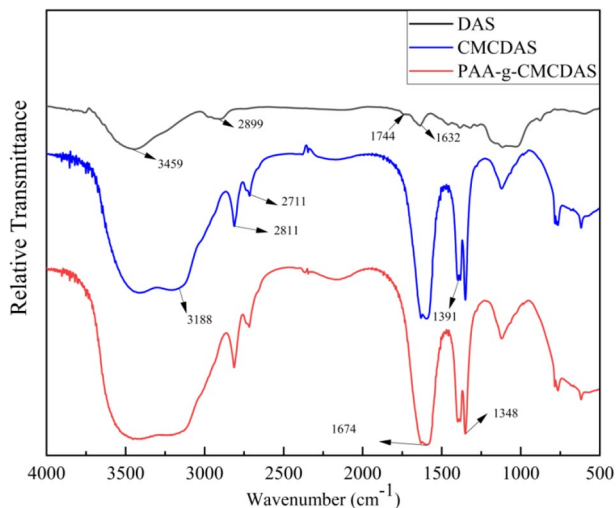**Fig. 5** Thermogravimetric curves of ST, DAS, CMCDAS and PAA-*g*-CMCDAS

Fig. 4 FT-IR spectra of DAS, CMCDAS and PAA-*g*-CMCDAS

exhibited good adsorption capacity for silver ions and its compounds.

The FTIR spectra of dialdehyde starch, CMCDAS and PAA-*g*-CMCDAS were shown in Fig. 4. The major peaks of
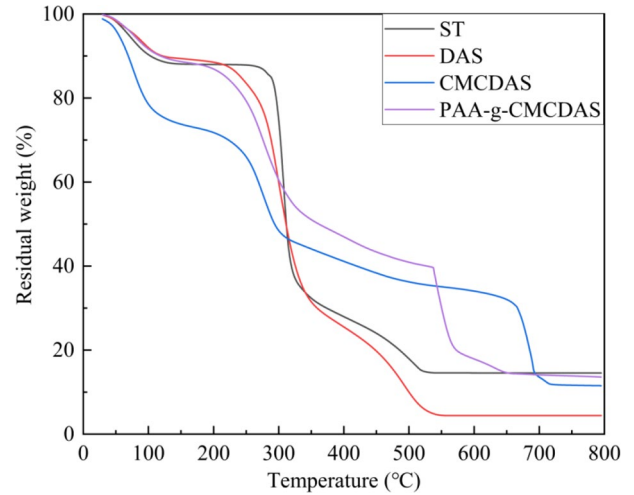
dialdehyde starch at 3459 cm^{-1}, 2899 cm^{-1} and 1632 cm^{-1} were always attributed to -OH, -CH_2 and C=O respectively [43]. From CMCDAS and PAA-*g*-CMCDAS, the peaks at 3188 cm^{-1}, 2811 cm^{-1} and 2711 cm^{-1} were always attributed to -OH and -CH in carboxymethyl chitosan; the peak at 1674 cm^{-1} was attributed to the stretching vibration peak of C=N according to the reaction of dialdehyde starch and carboxymethyl chitosan [44]; the peaks at 1324 cm^{-1} and 1412 cm^{-1} were attributed to the out of plane bending vibration peak of O-H and the stretching vibration of C=O [45, 46]. Therefore, CMCDAS was successfully cross-linked with acrylic acid.

There were three thermal degradation stages in the thermogravimetric curves of PAA-*g*-CMCDAS in Fig. 5. The first stage, below 190 ℃, with a weight loss of 10.2%, was always attributed to the evaporation of free water, bound water, carbon monoxide, carbon dioxide and ethanol on the surface of PAA-*g*-CMCDAS. The second stage, with a weight loss of 50.4% from 190 ℃ to 537 ℃, was always attributed to the shedding of hydroxyl, carboxyl and aldehyde groups, the cleavage of -C=N, the decomposition of pyranose and the Schiff base structure containing

unsaturated bonds and nitrogen atoms with lower energy [47]. The third stage, with a weight loss of 15.1% from 537 °C to 654 °C, was always attributed to the further shedding of carbonyl groups, hydroxyl groups and carboxyl groups, and the cleavage of the -C-N- bond. The thermal stability of PAA-*g*-CMCDAS was better compared to others. This may be caused by the crystal structure changes through the -C=N formation during the polymerization of carboxymethyl chitosan and acrylic acid. However, the C-N bond formed by polymerization with acrylic acid accelerated the collapse of its molecular structure [48]. At 800 °C, the residual amount of PAA-*g*-CMCDAS was 13.58%, which was higher than that of dialdehyde starch (4.43%) and CMCDAS (11.53%), but slightly lower than corn starch (14.56%).

The effect of acrylic acid on the specific surface area of CMCDAS was further studied by nitrogen isothermal adsorption and desorption experiments. As shown in Fig. 6, the samples all presented atypical type III curves, and the specific surface areas were 6.38 (ST), 8.56 (DAS),

11.51 (CMCDAS) and 14.15 (PAA-g-CMCDAS) $m^2 \cdot g^{-1}$, respectively. The pore size distribution range of the four samples was mainly concentrated between 2 and 8 nm, and there was a small number of micropores. After acrylic acid modification, the specific surface area of PAA-g-CMCDAS increased and its pores increased, which was beneficial to adhesion of silver ions on the surface of PAA-g-CMCDAS and improved the adsorption performance of PAA-g-CMCDAS for silver ions [49].

3.2 Adsorption performance

3.2.1 Effect of nitrogen content and acrylic acid content

The effect of the nitrogen content of PAA-*g*-CMCDAS on the Ag(I) adsorption was shown in Fig. 6a. The adsorption capacity of Ag(I) on PAA-*g*-CMCDAS with different nitrogen contents (1.23%, 2.464%, 3.10% and 3.472%) was 211.31 $mg \cdot g^{-1}$, 229.25 $mg \cdot g^{-1}$, 248.86 $mg \cdot g^{-1}$, 244.5
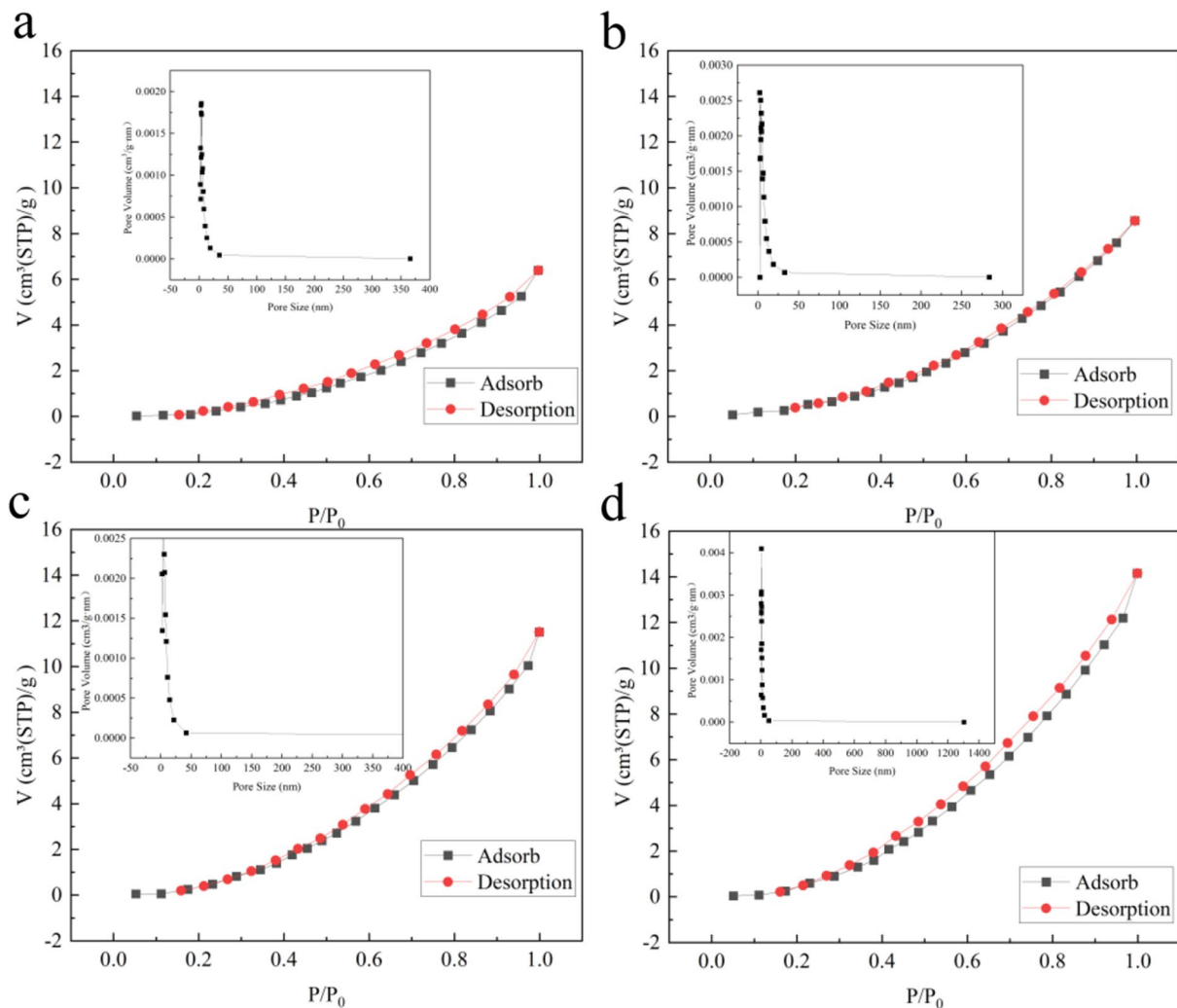

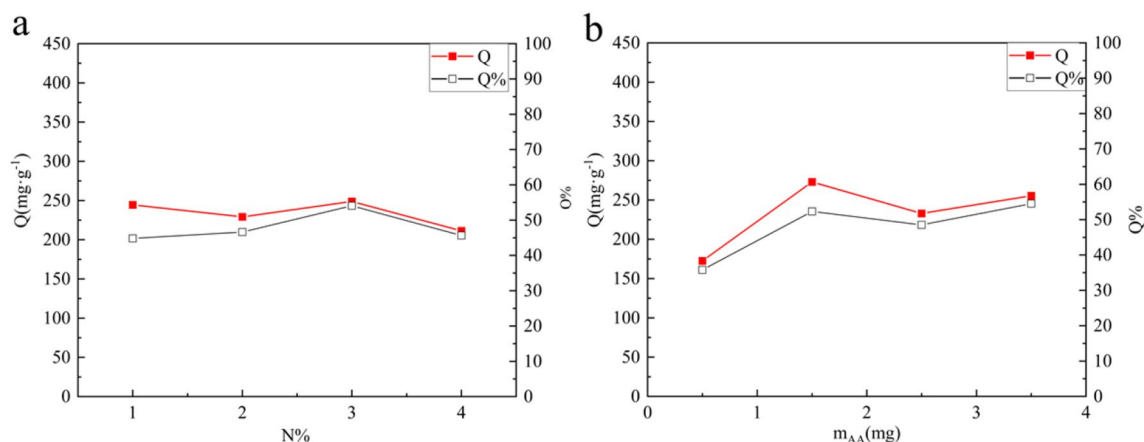**Fig. 6** The BET curves of ST (**a**), DAS (**b**), CMCDAS (**c**) and PAA-g-CMCDAS (**d**)

Fig. 7 Adsorption performance of Ag(I) on PAA-*g*-CMCDAS with different nitrogen content (**a**) and different acrylic acid content (**b**)

mg·g^{-1}, respectively, and the adsorption ratio of Ag(I) was 44.82%, 46.64%, 54.06% and 45.64%, respectively. The adsorption performance of Ag(I) on PAA-*g*-CMCDAS increased with increasing nitrogen content due to the chelation of metal ions and C=N. The adsorption performance of Ag(I) on the PAA-*g*-CMCDAS increased with the increasing content of acrylic acid (Fig. 6b). During the process of adding acrylic acid, the surface of CMCDAS became uneven, and then more attachment points on the surface of CMCDAS were obtained to adsorb Ag(I). Therefore, the content of nitrogen and the cross-linker acrylic acid had a significant effect on the adsorption performance.

3.2.2 Effect of adsorption time, temperature, dosage and initial concentration

The adsorption performance of Ag(I) on PAA-*g*-CMCDAS was studied, and the effect of adsorption time, temperature, dosage and initial concentrations were shown in Fig. 7a~d. The adsorption effect of Ag(I) on PAA-*g*-CMCDAS was up to 94.06% in 30 min and almost approached the adsorption equilibrium (Fig. 7a), which indicated that PAA-*g*-CMCDAS was fast adsorbent. The minimum silver ion removal efficiency was 41.44% at 20 °C, and the maximum was 55.75% at 40 °C (Fig. 7b). The 14.31% increase in removal efficiency indicated that the temperature is beneficial to the adsorption performance of the adsorbent [50]. The dosage study (Fig. 7c) showed that: (1) the maximum adsorption ratio of Ag(I) was 72.5% at 0.6 g adsorbent; (2) the adsorption effect increased with the increasing dosage of PAA-*g*-CMCDAS according to increasing surface area; (3) the adsorption capacity was saturated by Ag(I) on the surface of PAA-*g*-CMCDAS and the adsorption ratio slightly decreased which might be caused by the limit of temperature, nitrogen content and acrylic acid addition. The adsorption capacity and adsorption ratio of Ag(I) on PAA-*g*-CMCDAS

(Fig. 7d) gradually increased with the increase of the initial concentration, indicating that the initial concentration was benefit to adsorption capacity.

These results indicated that PAA-*g*-CMCDAS was an efficient fast adsorbent with lower insensitive to temperature, and the optimum conditions to adsorb Ag(I) contained the optimum adsorption time of 30 min, the optimum adsorption temperature of 40 °C, the optimum dosage of adsorbent 0.6 g and the higher initial concentration of Ag(I).

3.3 Adsorption kinetics

The adsorption equilibrium of the adsorbent and the mechanism of the adsorption process were determined by the adsorption kinetic equation, and then the adsorption process had to be optimized or extended. The quasi-frist-order kinetic and quasi-second-order kinetic model was used to verify the adsorption kinetics of Ag(I) on PAA-*g*-CMCDAS, and the model was usually expressed as the following equation (Eqs. 4 and 5) [51]:

$$\ln \frac{(Q_e - Q_t)}{Q_e} = -k_1 \tag{4}$$

$$\frac{t}{Q_t} = \frac{1}{k_2 Q_e^2} + \frac{1}{Q_e} t \tag{5}$$

Where Q_t and Q_e were the adsorption capacity of Ag(I) at time t and equilibrium, mg·g^{-1}, k_1 was the adsorption rate constant of the quasi-frist-order kinetic model, 1·min^{-1}. k_2 was the adsorption rate constant of the quasi-second-order kinetic model, g·(mg·min)$^{-1}$.

The adsorption kinetics of Ag(I) on PAA-*g*-CMCDAS was fitted (Fig. 8) and calculated using the quasi-frist-order kinetic and quasi-second-order kinetic model [52] (Table 1). The quasi-second-order kinetic parameters Q_e, k_2 and R^2

showed that the calculated theoretical adsorption capacity (Q_e) was close to the experimental adsorption capacity ($Q_{e.exp.}$) according to its R^2 almost close to 1. Therefore, the quasi-second-order was suitable for the adsorption of Ag(I), and the adsorption mechanism of Ag(I) by PAA-*g*-CMCDAS could be well simulated by a quasi-second-order kinetic model.

3.4 Adsorption isotherm

The adsorption isotherm was the relationship between the adsorption capacity and the equilibrium concentration at certain temperature [53–55], and the parameters calculated from different models would reveal the adsorption mechanism, surface properties and affinity of the adsorbents. Linear regression was a common method to determine the best fitting isotherm [51]. Therefore, the maximum adsorption capacity of the complete monolayer covered on the surface of PAA-*g*-CMCDAS could be estimated at 298.15 K by the Langmuir model equation and Freundlich model equation [56] (Eq. 6 and Eq. 7).

$$\frac{C_e}{Q_e} = \frac{C_e}{Q_{max}} + \frac{1}{K_L Q_{max}} \tag{6}$$

$$\log Q_e = \log K_F + \frac{1}{n_F} \log C_e \tag{7}$$

Where C_e is the equilibrium concentration, mg·g^{-1}; K_L is Langmuir constant, L·mg^{-1}, and Q_{max} is the maximum adsorption capacity, mg·g^{-1}, K_F is Freundlich constant, mg·g^{-1}. $1/n_F$ is adsorption intensity.

The adsorption isotherm of Ag(I) on PAA-*g*-CMCDAS was fitted (Fig. 9), and then the maximum adsorption capacity and other parameters was calculated using the Langmuir adsorption isotherm model [52] (Table 2). The higher value of R^2 (0.994) indicated that: (1) the adsorption isotherm of Ag(I) on PAA-*g*-CMCDAS was in accordance with the Langmuir adsorption model; (2) the adsorption of Ag(I) on PAA-*g*-CMCDAS belonged to monolayer adsorption and the adsorption capacity on the surface of PAA-*g*-CMCDAS was not uniform. According to the Freundlich model, the lower value of R^2 (0.8646) indicated that the adsorbent is more consistent with the Langmuir adsorption isotherm.

3.5 Reusability

The reusability of PAA-*g*-CMCDAS for Ag(I) was tested with optimum conditions and the adsorption capacity slightly decreased as the number of cycles increased (Fig. 10). The initial adsorption effect was up to 95.23% and the final adsorption effect was still up to 91.29% after five times

reuse. Compared to the silk fibroin adsorbent [57] (54.22% after four times reuse) and silver ion-imprinted magnetic adsorbent [58] (85% after six times reuse), our regenerated PAA-*g*-CMCDAS still had a high adsorption capacity for Ag(I), and the adsorption capacity slightly decreased after five times reuse. Therefore, PAA-*g*-CMCDAS was an efficient adsorbent for Ag(I) with good reusability and high adsorption performance.

3.6 Selectivity of PAA-g-CMCDAS

The adsorption performance of PAA-*g*-CMCDAS for single Ag(I), Ni(II), Co(II) and Cr(III) was shown in Fig. 11a, and the adsorption process was carried out at 0.05 mol·L^{-1} initial concentration, 313 K and 0.5 g dosage. The adsorption ratio of PAA-*g*-CMCDAS for Ag(I) was up to 93%, and the adsorption ratio for Ni(II), Co(II) and Cr(III) were 51%, 57% and 36% respectively [59].

The adsorption performance of PAA-*g*-CMCDAS for mixed metal ions was shown in Fig. 11b, and the adsorption process was carried out at 0.05 mol·L^{-1} initial concentration of each metal ion, 313 K and 0.5 g dosage. The adsorption ratio of PAA-*g*-CMCDAS for Ag(I) was 24%, which was higher than Cr(III) (17%), Co(II) (9%) and Ni(II) (6%), and the total removal efficiency of mixed metal ions was 58%. The results of the adsorption process for mixed metal ions indicated that PAA-*g*-CMCDAS had a preference for Ag(I) due to higher chelation between the monovalent Ag with a small radius and the outside negative C=N of PAA-*g*-CMC-DAS [60, 61]. Compared to the chitosan-coated magnetic adsorbent [62] (Q_{max}= 120 mg·g^{-1} in the mixed metal ions solution), PAA-*g*-CMCDAS was a specific adsorbent material for silver ions with good selectivity (See Fig. 12).

4 Conclusion

For the adsorption of silver ion, a novel environmental-friendly adsorbent (PAA-*g*-CMCDAS) was obtained from carboxymethyl chitosan (CMC), dialdehyde starch (DAS) and polyacrylic acid (PAA). DAS was modified by CMC to obtain carboxymethyl chitosan/dialdehyde starch (CMC-DAS) with -C=N groups. And, the acrylic graft CMCDAS (PAA-*g*-CMCDAS) was obtained by ionic copolymerization. The structure and morphology of the adsorbent was characterized by XRD, SEM, EDS, TGA, BET and FTIR. The optimum conditions for the obtained adsorbent were as follows, time was found to be 30 min, temperature was found to be 40 °C, the dosage was found to be 0.6 g and the higher initial concentration of silver ion. The adsorption process of silver ions conformed to Langmuir isotherm (R^2: 0.994) and the second-order kinetic model (R^2: 0.9999). The

Table 1 Kinetic parameters of PAA-*g*-CMCDAS (PAA: 1.5 g, N%: 3.1%)

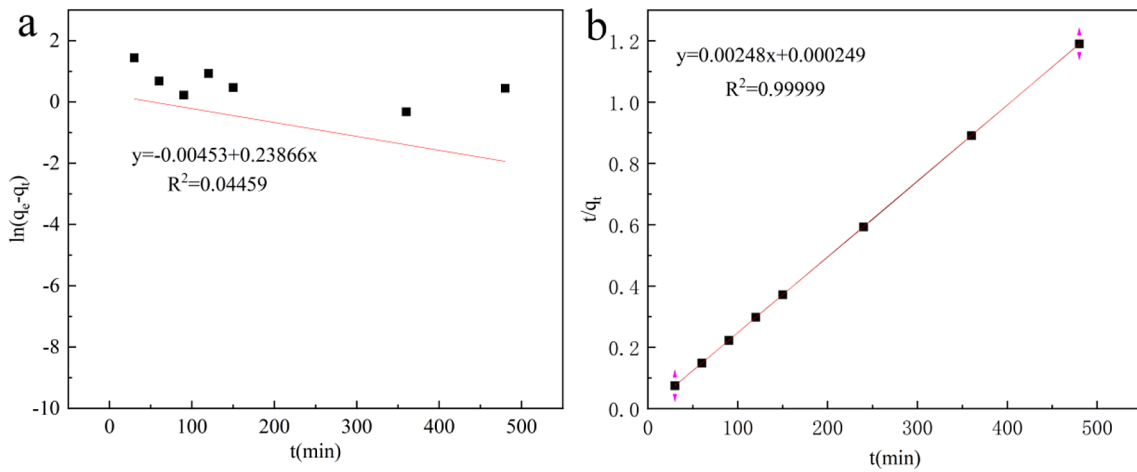|	Quasi-frist-order kinetic				Quasi-second-order kinetic			
T (K)	$Q_{e.exp.}$ (mg·g^{-1})	K_1 (1·min^{-1})	R^2	Q_e(mg·g^{-1})	$Q_{e.exp.}$ (mg·g^{-1})	K_2 (g·(mg·min)$^{-1}$)	R^2	Q_e(mg·g^{-1})
298.15	1.0045	0.9094	0.0446	1.6819	404.77	0.0247	0.9999	403.225

Fig. 9 Plot for quasi-frist-order kinetic (**a**) and quasi-second-order kinetic (**b**) of PAA-*g*-CMCDAS (PAA: 1.5 g, N%: 3.1%)

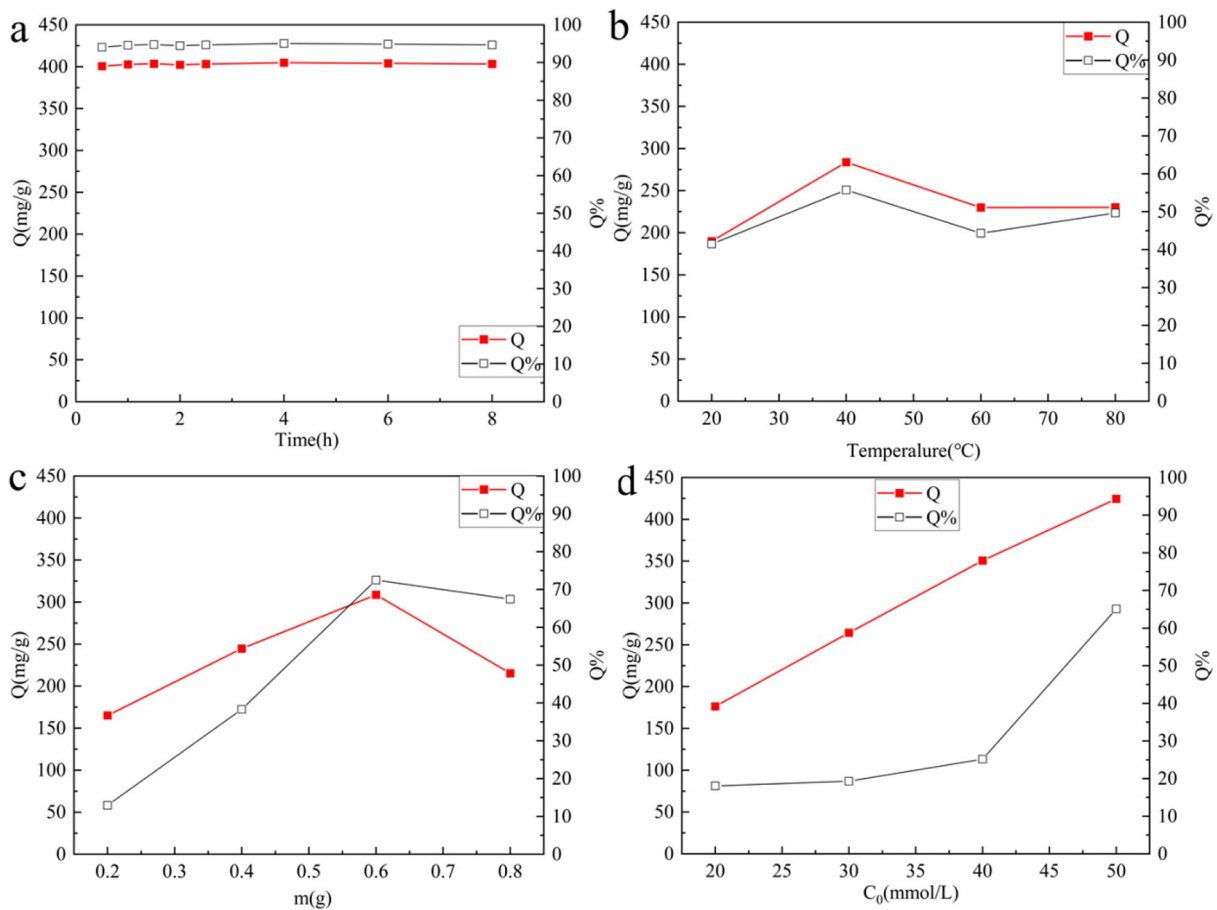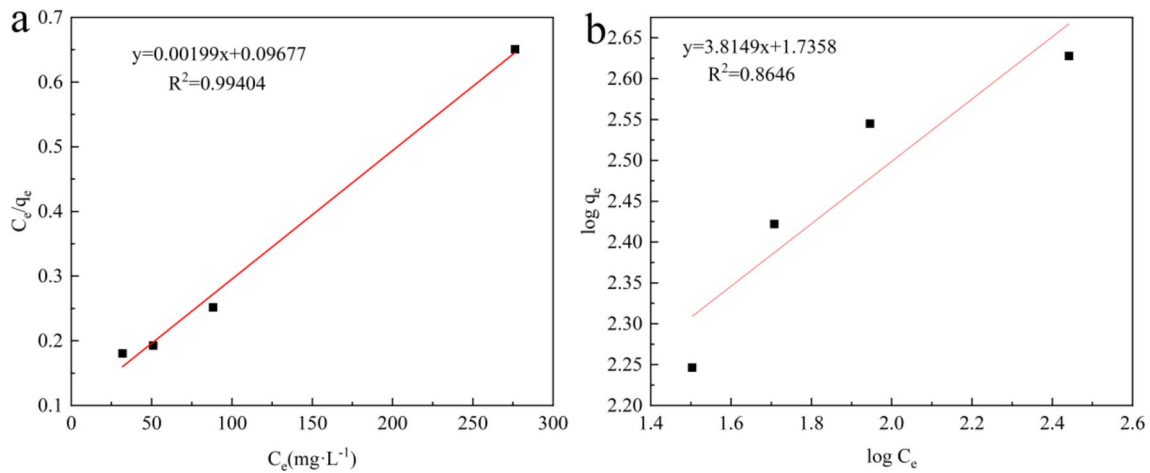**Fig. 8** Adsorption performance of Ag(I) on PAA-*g*-CMCDAS with different adsorption time (**a**), different temperature (**b**), different dosage (**c**) and different initial concentrations (**d**)

Table 2 Langmuir adsorption isotherm parameters of Ag(I) on PAA-*g*-CMCDAS (PAA: 1.5 g, N%: 3.1%)

	Langmuir			Freundlich		
T (K)	Q_{max} (mg·g^{-1})	K_L (L·mg^{-1})	R^2	K_F (1·mg^{-1})	$1/n_F$	R^2
298.15 K	502.512	0.0207	0.994	5.6734	0.2621	0.8646

Fig. 10 Langmuir adsorption isotherm (**a**) and Freundlich adsorption isotherm (**b**) of PAA-*g*-CMCDAS (PAA: 1.5 g, N%: 3.1%)
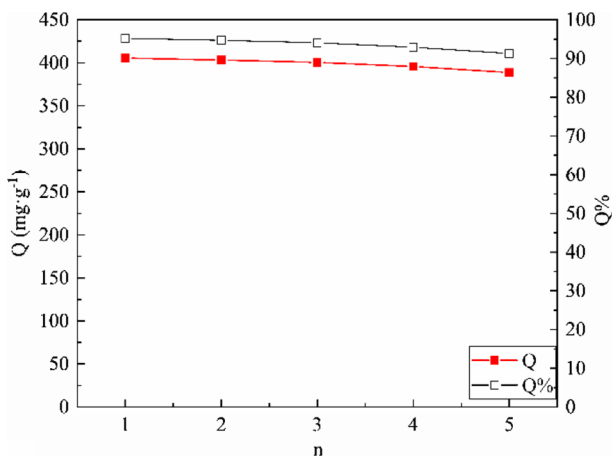
Fig. 11 Reusability of PAA-*g*-CMCDAS for Ag(I) (PAA:1.5 g, N%:3.1%)

maximum adsorption capacity for silver ions was 404.77 mg·g^{-1}, and the maximum removal efficiency was 95.05%. The adsorption amount was still 388.77 mg·g^{-1} and the removal efficiency was up to 91.29% after five times recycle. The removal efficiency of silver ions in mixed metal ions solution was 24.24% with the total removal efficiency of mixed metal ions 58%. Therefore, PAA-*g*-CMCDAS was an excellent silver ion adsorbent with good reusability.

Fig. 12 Adsorption performance of PAA-*g*-CMCDAS for metal ions (**a**: single metal ion; **b**: mixed metal ions) (PAA: 1.5 g, N%: 3.1%)
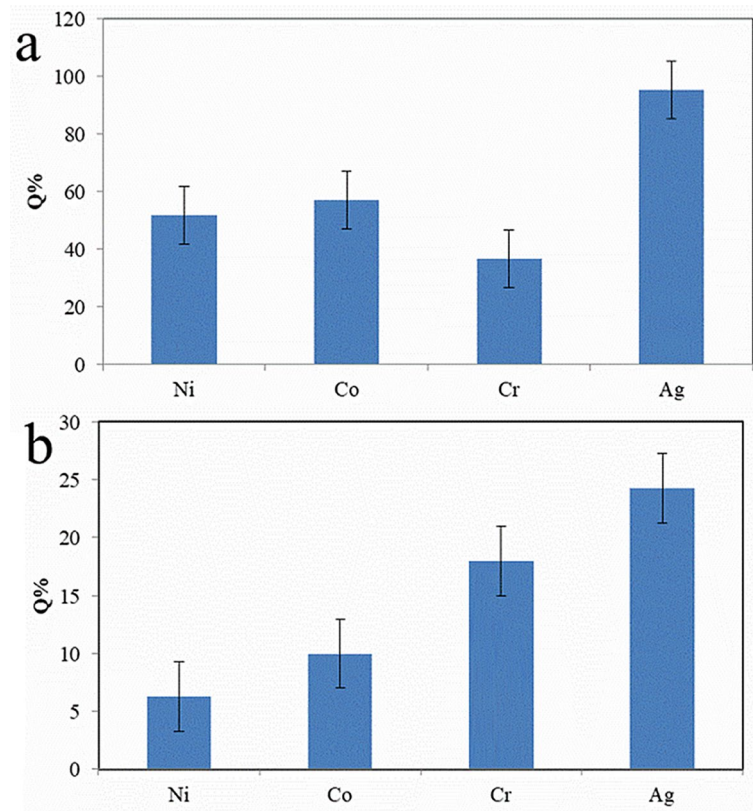
Declarations

Ethical approval Not applicable.

Competing interests Authors hereby declare that no conflicts of interest exist.

References

1. Sheng, X., Qin, C., Yang, B., Hu, X., Liu, C., Waigi, M.G., Li, X., Ling, W.: Metal cation saturation on montmorillonites facilitates the adsorption of DNA via cation bridging. Chemosphere. **235**, 670–678 (2019). https://doi.org/10.1016/j.chemosphere.2019.06.159

2. Zhang, P., Qin, C., Hong, X., Kang, G., Qin, M., Yang, D., Pang, B., Li, Y., He, J., Dick, R.P.: Risk assessment and source analysis of soil heavy metal pollution from lower reaches of Yellow River irrigation in China. Sci. Total Environ. **633**, 1136–1147 (2018). https://doi.org/10.1016/j.scitotenv.2018.03.228

3. Ansari, R., Delavar, A.F.: Application of poly 3-methylthiophene for removal of silver ion from aqueous solutions. J. Appl. Polym. Sci. **113**, 2293–2300 (2009). https://doi.org/10.1002/app.30239

4. Zhang, Y., Ye, A., Yao, Y., Yao, C.: A sensitive Near-Infrared fluorescent probe for Detecting Heavy Metal Ag^+ in Water samples. Sensors. **19** (2019). https://doi.org/10.3390/s19020247

5. Das, R., Giri, S., King Abia, A.L., Dhonge, B., Maity, A.: Removal of Noble Metal ions (Ag^+) by Mercapto Group-Containing Polypyrrole Matrix and Reusability of its Waste Material in Environmental Applications. ACS Sustain. Chem. Eng. **5**, 2711–2724 (2017). https://doi.org/10.1021/acssuschemeng.6b03008

6. Abbasi, E., Milani, M., Fekri Aval, S., Kouhi, M., Akbarzadeh, A., Tayefi Nasrabadi, H., Nikasa, P., Joo, S.W., Hanifehpour, Y., Nejati-Koshki, K., Samiei, M.: Silver nanoparticles: Synthesis methods, bio-applications and properties. Crit. Rev. Microbiol. **42**, 173–180 (2016). https://doi.org/10.3109/1040841X.2014.912200

7. Huang, Z.H., Jiang, X.L., Guo, D.W., Gu, N.: Controllable synthesis and Biomedical Applications of Silver nanomaterials. J. Nanosci. Nanotechnol. **11**, 9395–9408 (2011). https://doi.org/10.1166/jnn.2011.5317

8. Zhang, X.F., Liu, Z.G., Shen, W., Gurunathan, S.: Silver nanoparticles: Synthesis, characterization, properties, applications, and therapeutic approaches. Int. J. Mol. Sci. **17**, 1538 (2016). https://doi.org/10.3390/ijms17091534

9. Le Ouay, B., Stellacci, F.: Antibacterial activity of silver nanoparticles: A surface science insight. Nano Today. **10**, 339–354 (2015). https://doi.org/10.1016/j.nantod.2015.04.002

10. Huo, H., Su, H., Tan, T.: Adsorption of Ag^+ by a surface molecular-imprinted biosorbent. Chem. Eng. J. **150**, 139–144 (2009). https://doi.org/10.1016/j.cej.2008.12.014

11. Wu, F., Zhao, T., Yao, Y., Jiang, T., Wang, B., Wang, M.: Recycling supercapacitor activated carbons for adsorption of silver (I) and chromium (VI) ions from aqueous solutions.

Chemosphere. **238**, 124638 (2020). https://doi.org/10.1016/j.chemosphere.2019.124638

12. Lü, Q.F., Luo, J.J., Lin, T.T., Zhang, Y.Z.: Novel Lignin–Poly(N-methylaniline) composite sorbent for silver ion removal and recovery. ACS Sustain. Chem. Eng. **2**, 465–471 (2014). https://doi.org/10.1021/sc400475r

13. Fedorczyk, A., Skompska, M.: Quantitative studies of silver ions removal from aqueous solutions by poly(1,8-diaminocarbazole) films by means of electrochemical quartz crystal microbalance. Electrochim. Acta. **99**, 62–68 (2013). https://doi.org/10.1016/j.electacta.2013.03.087

14. Silva-Medeiros, F.V., Consolin-Filho, N., Xavier de Lima, M., Bazzo, F.P., Barros, M.A.S.D., Bergamasco, R., Tavares, C.R.G.: Kinetics and thermodynamics studies of silver ions adsorption onto coconut shell activated carbon. Environ. Technol. **37**, 3087–3093 (2016). https://doi.org/10.1080/09593330.2016.1176076

15. Beyler Çiğil, A., Aydın, Urucu, O., Birtane, H., Kahraman, M.V.: Cellulose/cysteine based thiol-ene UV cured adsorbent: removal of silver (I) ions from aqueous solution. Cellulose. 28, 6439–6448 (2021). https://doi.org/10.1007/s10570-021-03932-5

16. El-Shorbagy, H.G., El-Kousy, S.M., Elwakeel, K.Z., El-Ghaffar, M.A.A.: Eco-friendly Chitosan Condensation Adduct Resins for removal of toxic silver ions from Aqueous Medium. J. Ind. Eng. Chem. **100**, 410–421 (2021). https://doi.org/10.1016/j.jiec.2021.04.029

17. He, G., Wang, C., Cao, J., Fan, L., Zhao, S., Chai, Y.: Carboxymethyl Chitosan-Kaolinite composite hydrogel for efficient copper ions trapping. J. Environ. Chem. Eng. **7**, 102953 (2019). https://doi.org/10.1016/j.jece.2019.102953

18. Medeiros Borsagli, F.G.L., Mansur, A.A.P., Chagas, P., Oliveira, L.C.A., Mansur, H.S.: O-carboxymethyl functionalization of chitosan: Complexation and adsorption of cd (II) and cr (VI) as heavy metal pollutant ions. Reactive Funct. Polym. **97**, 37–47 (2015). https://doi.org/10.1016/j.reactfunctpolym.2015.10.005

19. Charpentier, T.V.J., Neville, A., Lanigan, J.L., Barker, R., Smith, M.J., Richardson, T.: Preparation of magnetic Carboxymethylchitosan nanoparticles for Adsorption of Heavy Metal ions. Acs Omega. **1**, 77–83 (2016). https://doi.org/10.1021/acsomega.6b00035

20. Wasikiewicz, J.M., Nagasawa, N., Tamada, M., Mitomo, H., Yoshii, F.: Adsorption of metal ions by carboxymethylchitin and carboxymethylchitosan hydrogels. Nuclear instruments and methods. Phys. Res. Sect. B: Beam Interact. Mater. Atoms. **236**, 617–623 (2005). https://doi.org/10.1016/j.nimb.2005.04.053

21. Ifthikar, J., Jiao, X., Ngambia, A., Wang, T., Khan, A., Jawad, A., Xue, Q., Liu, L., Chen, Z.: Facile One-Pot synthesis of sustainable Carboxymethyl Chitosan – Sewage Sludge Biochar for Effective Heavy Metal Chelation and Regeneration. Bioresour. Technol. **262**, 22–31 (2018). https://doi.org/10.1016/j.biortech.2018.04.053

22. Nitayaphat, W., Jintakosol, T.: Removal of silver(I) from aqueous solutions by chitosan/bamboo charcoal composite beads. J. Clean. Prod. **87**, 850–855 (2015). https://doi.org/10.1016/j.jclepro.2014.10.003

23. Gupta, A.D., Rawat, K.P., Bhadauria, V., Singh, H.: Recent trends in the application of modified starch in the adsorption of heavy metals from water: A review. Carbohydr. Polym. **269**, 117763 (2021). https://doi.org/10.1016/j.carbpol.2021.117763

24. Akinterinwa, A., Reuben, U., Atiku, J.U., Adamu, M.: Focus on the removal of lead and cadmium ions from aqueous solutions using starch derivatives: A review. Carbohydr. Polym. **290**, 119463 (2022). https://doi.org/10.1016/j.carbpol.2022.119463

25. Krystyjan, M., Khachatryan, G., Grabacka, M., Krzan, M., Witczak, M., Grzyb, J., Physicochemical, W.L.: Bacteriostatic, and Biological Properties of Starch/Chitosan Polymer composites modified by Graphene Oxide, designed as New

26. Liu, Q., Li, F., Lu, H., Li, M., Liu, J., Zhang, S., Sun, Q., Xiong, L.: Enhanced dispersion stability and heavy metal ion adsorption capability of oxidized starch nanoparticles. Food Chem. **242**, 256–263 (2018). https://doi.org/10.1016/j.foodchem.2017.09.071

27. Ibrahim, B.M., Fakhre, N.A.: Crown ether modification of starch for adsorption of heavy metals from synthetic wastewater. Int. J. Biol. Macromol. **123**, 70–80 (2019). https://doi.org/10.1016/j.ijbiomac.2018.11.058

28. Para, A.: Complexation of metal ions with dioxime of dialdehyde starch. Carbohydr. Polym. **57**, 277–283 (2004). https://doi.org/10.1016/j.carbpol.2004.05.005

29. Para, A., Karolczyk-Kostuch, S.: Semicarbazone of starch dialdehyde and its complexes with metal ions. Carbohydr. Polym. **48**, 55–60 (2002). https://doi.org/10.1016/S0144-8617(01)00211-9

30. Yin, Q.F., Ju, B.Z., Zhang, S.F., Wang, X.B., Yang, J.Z.: Preparation and characteristics of novel dialdehyde aminothiazole starch and its adsorption properties for Cu (II) ions from aqueous solution. Carbohydr. Polym. **72**, 326–333 (2008). https://doi.org/10.1016/j.carbpol.2007.08.019

31. Antonkiewicz, J., Para, A.: The use of dialdehyde starch derivatives in the phytoremediation of soils contaminated with heavy metals. Int. J. Phytoremediation. **18**, 245–250 (2016). https://doi.org/10.1080/15226514.2015.1078771

32. Li, Z., Wang, X., Miao, J., Xing, L., Zhang, S.: Antibacterial activity of Dodecylamine Dialdehyde Starch Schiff base derivatives. Starch - Stärke. **74**, 2100178 (2022). https://doi.org/10.1002/star.202100178

33. Peidayesh, H., Ahmadi, Z., Khonakdar, H.A., Abdouss, M., Chodák, I.: Fabrication and properties of thermoplastic starch/montmorillonite composite using dialdehyde starch as a cross-linker. Polym. Int. **69**, 317–327 (2020). https://doi.org/10.1002/pi.5955

34. Lv, Q., Hu, X., Zhang, X., Huang, L., Liu, Z., Sun, G.: Highly efficient removal of trace metal ions by using poly(acrylic acid) hydrogel adsorbent. Mater. Design. **181**, 107934 (2019). https://doi.org/10.1016/j.matdes.2019.107934

35. Hu, L.Q., Dai, L., Liu, R., Si, C.L.: Lignin-graft-poly(acrylic acid) for enhancement of heavy metal ion biosorption. J. Mater. Sci. **52**, 13689–13699 (2017). https://doi.org/10.1007/s10853-017-1463-1

36. Zhao, B., Jiang, H., Lin, Z., Xu, S., Xie, J., Zhang, A.: Preparation of acrylamide/acrylic acid cellulose hydrogels for the adsorption of heavy metal ions. Carbohydr. Polym. **224**, 115022 (2019). https://doi.org/10.1016/j.carbpol.2019.115022

37. Chen, Y., Hao, Y.C., Kou, T., Li, Q., Gao, Q.Y.: Preparation and emulsification properties of dialdehyde starch nanoparticles. Food Chem. **286**, 467–474 (2019). https://doi.org/10.1016/j.foodchem.2019.01.188

38. Hou, Q., Liu, W., Liu, Z., Duan, B., Bai, L.: Characteristics of antimicrobial fibers prepared with wood periodate oxycellulose. Carbohydr. Polym. **74**, 235–240 (2008). https://doi.org/10.1016/j.carbpol.2008.02.010

39. Zhou, X., Essawy, H.A., Mohamed, M.F., Ibrahim, H.S., Ammar, N.S.: Grafting polymerization of acrylic acid onto chitosan-cellulose hybrid and application of the graft as highly efficient ligand for elimination of water hardness: Adsorption Isotherms, kinetic modeling and regeneration. J. Environ. Chem. Eng. **6**, 2137–2147 (2018). https://doi.org/10.1016/j.jece.2018.03.022

40. Nitayaphat, W., Jintakosol, T.: Adsorption of Ag (I) from Aqueous solutions using regenerated Silk Fibroin Adsorbent beads. J. Nat. Fibers. 1–13 (2020). https://doi.org/10.1080/15440478.2020.1848697

41. Wongsagon, R., Shobsngob, S., Varavinit, S.: Preparation and Physicochemical Properties of Dialdehyde Tapioca Starch.

Bionanomaterials. Polym. Adv. Technol. **13** (2021). https://doi.org/10.3390/polym13142327

Starch - Stärke. **57**, 166–172 (2005). https://doi.org/10.1002/star.200400299

42. Haroon, M., Yu, H., Wang, L., Ullah, R.S., Haq, F., Teng, L.: Synthesis and characterization of carboxymethyl starch-g-poly-acrylic acids and their properties as adsorbents for ammonia and phenol. Int. J. Biol. Macromol. **138**, 349–358 (2019). https://doi.org/10.1016/j.ijbiomac.2019.07.046

43. Zhang, L., Liu, J., Zheng, X., Zhang, A., Zhang, X., Tang, K.: Pullulan dialdehyde crosslinked gelatin hydrogels with high strength for biomedical applications. Carbohydr. Polym. **216**, 45–53 (2019). https://doi.org/10.1016/j.carbpol.2019.04.004

44. Chen, L., Hao, H., Zhang, W., Shao, Z.: Adsorption mechanism of copper ions in aqueous solution by chitosan–carboxymethyl starch composites. J. Appl. Polym. Sci. **137**, 48636 (2020). https://doi.org/10.1002/app.48636

45. Luo, C., Li, M., Yuan, R., Yang, Y., Lu, Z., Ge, L.: Biocompatible Self-Healing Coating based on Schiff Base for promoting adhesion of Coral cells. ACS Appl. Bio Mater. **3**, 1481–1495 (2020). https://doi.org/10.1021/acsabm.9b01113

46. Chen, X., Li, Y., Qiu, Y.-L., Zhang, G.-L., Hao, H., Hou, H.-M., Bi, J.: Amino carboxymethyl chitosan//dialdehyde starch/polyvinyl alcohol double-layer film loaded with ε-polylysine. Food Chem. **428**, 136775 (2023). https://doi.org/10.1016/j.foodchem.2023.136775

47. Liu, Y., Yang, L., Ma, C., Zhang, Y.: Thermal behavior of Sweet Potato Starch by Non-isothermal Thermogravimetric Analysis. Materials. **12**, 699 (2019). https://doi.org/10.3390/ma12050699

48. Pasini, S.M., Batistella, M.A., de Souza, S.M.A.G.U., Wang, J., Hotza, D., de Souza: A.A.U. Thermal degradation and flammability of TiO2–polyetherimide nanocomposite fibers. Polym. Bull. **77**, 4937–4958 (2020). https://doi.org/10.1007/s00289-019-02970-1

49. Bashiri, H., Nesari, S., Sarabadan, M.: Microwave assistant production of a high performance adsorbent from rice husk. Korean J. Chem. Eng. **37**, 240–248 (2020). https://doi.org/10.1007/s11814-019-0446-0

50. Zhang, X., Yang, S., Yu, B., Tan, Q., Zhang, X., Cong, H.: Advanced Modified Polyacrylonitrile membrane with enhanced Adsorption Property for Heavy Metal Ions. Sci. Rep. **8**, 1260 (2018). https://doi.org/10.1038/s41598-018-19597-3

51. Kiani, G.: High removal capacity of silver ions from aqueous solution onto Halloysite nanotubes. Appl. Clay Sci. **90**, 159–164 (2014). https://doi.org/10.1016/j.clay.2014.01.010

52. Taty-Costodes, V.C., Fauduet, H., Porte, C., Delacroix, A.: Removal of cd(II) and pb(II) ions, from aqueous solutions, by adsorption onto sawdust of Pinus sylvestris. J. Hazard. Mater. **105**, 121–142 (2003). https://doi.org/10.1016/j.jhazmat.2003.07.009

53. Kalam, S., Abu-Khamsin, S.A., Kamal, M.S., Patil, S.: Surfactant Adsorption isotherms: A review. Acs Omega. **6**, 32342–32348 (2021). https://doi.org/10.1021/acsomega.1c04661

54. Chang, C.K., Tun, H., Chen, C.C.: An activity-based formulation for Langmuir adsorption isotherm. Adsorption. **26**, 375–386 (2020). https://doi.org/10.1007/s10450-019-00185-4

55. Al-Ghouti, M.A., Da'ana: D.A. guidelines for the use and interpretation of adsorption isotherm models: A review. J. Hazard. Mater. **393**, 122383 (2020). https://doi.org/10.1016/j.jhazmat.2020.122383

56. Huang, S.H., Chen, D.H.: Rapid removal of heavy metal cations and anions from aqueous solutions by an amino-functionalized magnetic nano-adsorbent. J. Hazard. Mater. **163**, 174–179 (2009). https://doi.org/10.1016/j.jhazmat.2008.06.075

57. Nitayaphat, W., Jintakosol, T.: Adsorption of Ag (I) from Aqueous solutions using regenerated Silk Fibroin Adsorbent beads. J. Nat. Fibers. **19**, 3365–3377 (2022). https://doi.org/10.1080/15440478.2020.1848697

58. Zhang, M., Wang, H., Wu, Y., Yu, X.: Silver ion-imprinted magnetic adsorbent hyphenated to single particle-ICP-MS for separation and analysis of dissolved silver and silver nanoparticles in antibacterial gel extracts. Anal. Chim. Acta. **1279**, 341846 (2023). https://doi.org/10.1016/j.aca.2023.341846

59. Zhang, L., Zhang, G., Wang, S., Peng, J., Cui, W.: Sulfoethyl functionalized silica nanoparticle as an adsorbent to selectively adsorb silver ions from aqueous solutions. J. Taiwan Inst. Chem. Eng. **71**, 330–337 (2017). https://doi.org/10.1016/j.jtice.2017.01.001

60. Fu, L., Zhang, L., Wang, S., Peng, J., Zhang, G.: Selective adsorption of Ag^+ by silica nanoparticles modified with 3-Amino-5-mercapto-1,2,4-triazole from aqueous solutions. J. Mol. Liq. **241**, 292–300 (2017). https://doi.org/10.1016/j.molliq.2017.06.028

61. Shao, P., Chang, Z., Li, M., Lu, X., Jiang, W., Zhang, K., Luo, X., Yang, L.: Mixed-valence molybdenum oxide as a recyclable sorbent for silver removal and recovery from wastewater. Nat. Commun. **14**, 1365 (2023). https://doi.org/10.1038/s41467-023-37143-2

62. Huang, Y., Wu, Y., Ding, W., Sun, Q., Hu, C., Liu, B., Liu, H., Zheng, H.: Anion-synergistic adsorption enhances the selective removal of silver ions from complex wastewater by chitosan-coated magnetic silica core-shell nanoparticles. J. Clean. Prod. **339**, 130777 (2022). https://doi.org/10.1016/j.jclepro.2022.130777